Stacking, correlations and electronic dispersion in the photoexcited state of 1T-TaS_2

Jingwei Dong[1], Dongbin Shin[2,3], Ernest Pastor[4], Tobias Ritschel[5], Laurent Cario[6], Zhesheng Chen[7], Weyain Qi[1], Romain Grasset[1], Marino Marsi[7], Amina Taleb[8], Noejung Park[9], Angel Rubio[3], Luca Perfetti[1] and Evangelos Papalazarou[7]

[1] *Laboratoire des Solides Irradiés, CEA/DRF/lRAMIS, Ecole Polytechnique, CNRS, Institut Polytechnique de Paris, F-91128 Palaiseau, France*

[2] *Department of Physics and Photon Science, Gwangju Institute of Science and Technology (GIST), Gwangju 61005, Republic of Korea*

[3] *Max Planck Institute for the Structure and Dynamics of Matter and Center for Free-Electron Laser Science, Luruper Chaussee 149, 22761 Hamburg, Germany*

[4] *Institute of Advanced Materials (INAM), Universitat Jaume I, Avenida de Vicent Sos Baynat, s/n 12006, Castelló, Spain*

[5] *Institut für Festkörper- und Materialphysik, Technische Universität Dresden, 01069, Dresden, Germany*

[6] *Nantes Université, CNRS, Institut des Matériaux de Nantes Jean Rouxel, IMN, F-44000 Nantes, France*

[7] *Université Paris-Saclay, CNRS, Laboratoire de Physique des Solides, 91405 Orsay Cedex, France*

[8] *Synchrotron SOLEIL, Saint Aubin BP 48, Gif-sur-Yvette F-91192, France and*

[9] *Department of Physics, Ulsan National Institute of Science and Technology (UNIST), UNIST-gil 50, Ulsan 44919, Korea*

Here we perform angle and time-resolved photoelectron spectroscopy on the commensurate Charge Density Wave phase of 1T-TaS_2. Data with different probe pulse polarization are employed to map the dispersion of electronic states below or above the chemical potential. The experimental results are compared to Density-Functional Theory calculations with a self-consistent evaluation of the coulomb repulsion. Both out-of-plane dimerization and electronic correlations must be included in order to obtain good agreement with the experimental data. Upon Photoexcitation, the fluctuations of CDW order erase the band dispersion near to the chemical potential and halve the charge gap size. This transient phase sets within half a period of the coherent lattice motion and is likely favored by strong electronic correlations.

PACS numbers:

The transition metal 1T-TaS_2 is a layered insulator with a rich phase diagram as a function of pressure and temperature. Its broken symmetry phases include incommensurate, nearly commensurate, and commensurate Charge Density Waves (CDWs)[1]. Within each layer, the Ta lattice undergoes a periodic distortion in which 13 Ta ions form clusters with the motif of a Star-of-David (SD)[2]. These clusters have an odd filling and lock-in to a Commensurate CDW (C-CDW) below 180 K. The observed insulating behavior of the C-CDW phase is generally attributed to the Mott localization of the electron in the highest occupied state of SDs[3–5]. A superconducting phase develops upon pressure[6], whereas metastable states can be reached by the application of laser[7] or current pulses[8,9]. These entwined orders emerge from the interplay of electron-phonon and electron-electron interactions, both being particularly strong in this dichalcogenide.

Although widely believed to be a Mott insulator, the commensurate CDW phase also features an interlayer stacking with SDs dimerization. The doubling of unit cell along the c-axis direction has been confirmed by many different experiments as X-Ray Diffraction (XRD)[10], Angle-Resolved Photoelectron Spectroscopy (ARPES)[11–13], Scanning Tunneling Microscopy (STM)[14] and Low Energy Electron Diffraction (LEED)[15]. As shown in the structural model in Fig. 1A, there are two possible stacking orders; Top Aligned (A) and Laterally displaced (L) with a vector of magnitude $2a$. The ground dimerized geometry of TaS_2 shows alternating stacking between A and L configurations, called AL stacking[10]. With this stacking configuration, two possible cleavage planes have been observed by local probes, one leaving an intact bilayer at the surface and the other with an undimerized topmost layer[14].

By hosting an even number of electrons, the dimerized unit cell of the commensurate CDW cannot be a pure Mott phase. As in the case of VO_2[16], the instability of 1T-TaS_2 results from the interplay of strong correlations and structural distortion. This duality gave origin to several works, addressing the Slater-towards-Mott character of the ground state. Recent calculations revised the strength of Coulomb repulsion in this family of compounds and highlighted the strong effects that electronic interactions have on the band structure of 1T-TaS_2[17]. Notable arguments backing this point of view are: the Mott gap observed in monolayer 1T-$TaSe_2$[31], the high sensitivity of the insulating state to non-isoelectronic substitution[18], and the dynamical response of electronic states upon photoexcitation[19,20]. In particular, the ultrafast collapse of the gap at relatively low excitation density has often been availed as the major indication of strong electron-electron interaction[19,21,22].

This work reports time-resolved ARPES measurement on high-quality single crystals of 1T-TaS_2 in the insulating C-CDW phase. By making use of different polarizations of the probe pulse, we are able to visualize the dispersion of electronic states below and above the chem-

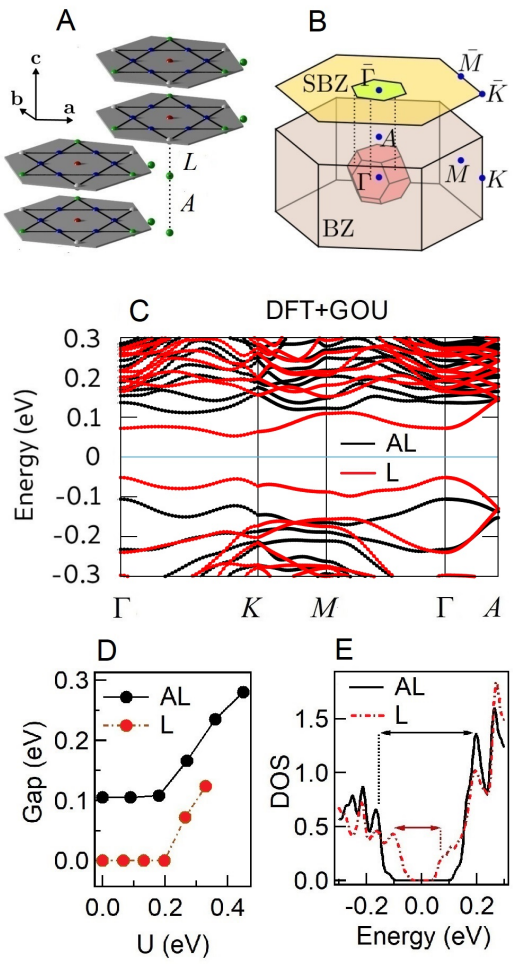

FIG. 1: A) Unit cell of the AL stacking in the commensurate CDW phase of 1T-TaS_2 B) Bulk Brillouin Zone (BZ) and surface Brillouin Zone (SBZ) of the undistorted and distorted structure of 1T-TaS_2. The high symmetry points Γ, A, K, M, L refer to BZ of the undistorted structure and $\bar{\Gamma}$, $\bar{M}$, $\bar{K}$ are the respective projections on the SBZ. C) Band structure of the AL stacking (black) and L stacking (Red) calculated by DFT+GOU theory. The self-consistent $\overline{U}_{AL} = 0.45$ eV and $\overline{U}_L = 0.33$ eV are obtained via the ABCN0 method. D) Electronic gap calculated by the DFT+GOU theory as a function of U potential for the AL and L stacking. The largest U value corresponds to the self-consistent finding $U = \overline{U}$. E) Density of electronic states of the AL and L stacking calculated by self-consistent DFT+GOU.

ical potential. The experimental data are compared with state-of-the-art Density Functional Theory calculations with the Generalized Orbital U (DFT+GOU)[17]. The Coulomb $\overline{U}$ of a SD cluster is self-consistently calculated via the ACBN0 method. Our results indicate that both stacking order and electronic correlations are essential to reproduce the correct gap size. Moreover, time-resolved ARPES data acquired with S polarized probe disclose novel aspects of the photoinduced phase transition. The pump pulse erases the band dispersion and halves the gap magnitude within half a period of the coherent CDW motion. Besides the oscillations of CDW amplitude, We propose that photoexcitation also engenders local variations of dimerization, orbital filling, and $\overline{U}$ potential. The combination of these effects triggers the melting of the Mott-Peierls gap.

Figure 1B shows the unreconstructed Brillouin Zone (BZ) of primitive 1T-TaS_2 lattice and the reconstructed BZ of a periodic structure with C-CDW lattice modulation and AL staking. We performed DFT calculation using the Quantum ESPRESSO package with PBE-type functional. Wave functions are obtained via the projector-augmented plane wave method and a basis set with a cutoff energy of 60 Ry. The lattice constant for bulk 1T-TaS_2 are $a = 3.36$ Å, $c = 6.03$ Å and a $3 \times 3 \times 6$ k-point mesh samples the Brillouin zone. In the case of DFT + GOU, the $\overline{U}$ potential of a SD cluster is obtained self consistently via the ACBN0 method, where $\overline{U}$ and $\overline{J}$ parameters are determined through the theory of screened Hartree-Fock exchange potential in a correlated subspace. The band structure calculated by $DFT{+}GOU$ for AL and L stacking is shown in Fig. 1C. Electronic correlations strongly affect the electronic states, stabilizing the insulating phase. Figure 1D shows the direct gap Δ as a function of Coulomb repulsion U for the case of dimerized AL stacking and undimerized L stacking. In the case of AL stacking, the gap is $\Delta = 0.1$ eV if correlations are ignored ($U = 0$) while it increases up to $\Delta_{AL} = 0.28$ eV when U is equal to the self-consistent $\overline{U}_{AL} = 0.45$ eV. Instead, for pure L stacking the system is metallic for $U \leq 0.2$ eV and attains a gap $\Delta_L = 0.12$ eV when U is equal to the self consistent $\overline{U}_L = 0.33$ eV. Figure 1E plots the Density Of electronic States for AL and L stacking. The distance between the nearest peaks below and above the chemical potential (arrows on the figure) is roughly 30% percent larger than the gap value, corresponding to 0.36 eV for the AL case and 0.17 eV for the L case. These values agree with the scanning tunneling spectroscopy spectra measured on the AL, and L termination of the 1T-TaS_2 surface[14]. We evince that the $DFT + GOU$ calculations provide a better description of the electronic states than simple DFT. Remark that also other methods, such as the $GW - EDMFT$, have been recently able to account for correlation and dimerization of the 1T-TaS_2 groundstate[23]. Compared to $GW - EDMFT$ calculations, the $DFT + GOU$ method has both advantages and drawbacks: it does not retrieve the full spectral function but is fully *ab-initio* (no adjustable parameters) and can treat the multiband problem without restricting the Hilbert space to one effective orbital.

Time-resolved ARPES experiments have been carried out on a single crystal cleaved at room temperature and subsequently cooled to 135 K. The sample is photoexcited by a pump pulse of 300 μJ/cm^2 and centered at 1.55 eV[25]. If not differently specified, the photoelectrons are emitted by a delayed pulse at 6.3 eV, with a bandwidth of 30 meV and a duration of 170 fs. This parameter

choice is an optimal tradeoff between energy and temporal resolution for this specific experiment. In our setup (see Fig. 2A), the P polarization corresponds to an electric field having equal projections along the $\overline{\Gamma}-\overline{M}$ and the c-axis direction. Figure 2B,C shows photoelectron intensity maps acquired along the $\overline{\Gamma}-\overline{M}$ direction of the unreconstructed Surface Brillouin Zone (SBZ), with P polarized probe and pump-probe delay of -200 fs (panel B) or 0 fs (panel C). An internal reference of pump-probe cross-correlation is obtained by monitoring the temporal evolution of states well above the chemical potential (see Fig. 2E.

Due to the interplay of electron-electron interaction and stacking order, we refer to the states below or above the chemical potential (zero of energy axis) as Lower Mott-Peierls Band (LMPB) and Upper Mott-Peierls band (UMPB), respectively. Since the UMPB also displays a sizable c-axis dispersion, the spectral weight redistribution of the ARPES intensity varies with probe photon energy[24]. In the case of 6.3 eV probe photons, the LMPB peaks near -0.2 eV for $k_{||} = 0.2$ Å^{-1} and moves towards the chemical potential for $k_{||} \to 0$. This electronic structure is expected for $k_\perp$ projections where the energy distance between LMPB and UMPB becomes minimal[12,24]. Figure 2D displays the temporal evolution of the photoelectron signal integrated around $\overline{\Gamma}$. Upon photoexcitation, the spectral weight is suddenly transferred to higher energy, inducing the ultrafast filling of the gap. A displacive excitation of SDs breathing mode provokes large and periodic modulations of the LMPB peak. The frequency of this symmetric mode corresponds to 2.4 THz, which is in good agreement with the value extracted via stimulated Raman scattering[26], electron diffraction[27] and previous time resolved ARPES results[19,21,22].

New insights into the structure of electronic states can be obtained by collecting photoelectron maps with S polarized photons. As shown in the sketch of Fig. 2A, the electric field of S polarized light lies in the surface plane and is perpendicular to the analyzer slits. The essential role played by the probe polarization on the ARPES maps of 1T-TaS_2 has been overlooked in previous experiments[19–22,28] while it deserves special care in the data analysis. Depending on the lattice structure, a dichroic effect can indeed modulate the photoemission intensity of electronic states, either exalting or hindering the visibility of specific features. Similar observations have been recently done in black phosphorous, where the linear dichroism is discussed in a pseudospin representation[29]. These effects are as drastic in 1T-TaS_2 as they are in black phosphorous (see the intensity maps at photon energy 96 eV and shown in the supplementary information file). As shown in Fig. 3A, the S polarization strongly reduces the emission intensity of the LMPB while increasing the emission intensity of states above the chemical potential. It is now possible to see that an Upper Mott Peierls Band (UMPB) is transiently occupied by the pump laser pulse. Our experimental observation

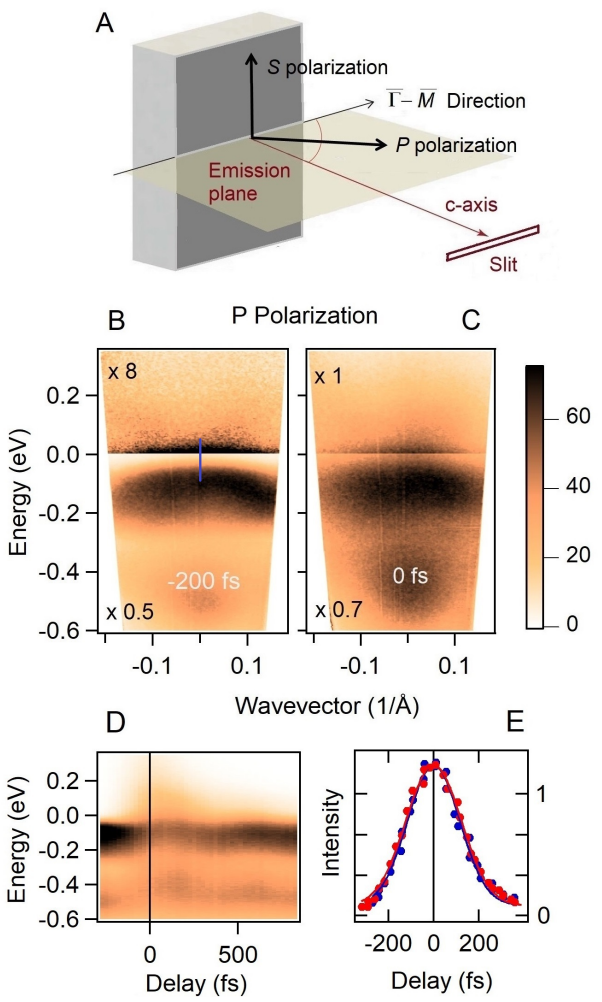

FIG. 2: A) Orientation of the P and S polarization in the experimental geometry of the present work. The electric field of P polarized light forms an angle of 45° both with the $\overline{\Gamma}-\overline{M}$ direction and the c-axis direction. B-C) Photoelectron intensity map acquired with ***P* probe polarization** along the $\overline{\Gamma}-\overline{M}$ direction for pump-probe delay of -200 fs (panel B) and 0 fs (panel C). The intensities above and below the Fermi level have been multiplied by rescaling factors in order to better visualize the electronic states with respect to a fixed color scale. The blue line in panel B stands for the electronic gap size. D) Photoelectron intensity acquired with P probe polarization, integrated in the wavevector interval [-0.1,0.1] Å^{-1}) and plotted as a function of pump-probe delay. E) Cross-correlation between pump and probe pulse obtained by extracting the photoelectron signal located 0.4 eV above the Fermi level. Blue and red circles correspond to P and S probe polarization, respectively.

is consistent with the orbital d_{z^2} character of the LMPB and a mixed $d_{z^2} - d_{x^2-y^2}$ character of the UMPB (see supplementary information file). Indeed the dipolar moment leading to photoelectrons emission points along the c-axis for d_{z^2} orbital while it lies in-plane for the $d_{x^2-y^2}$ one.

As shown in Fig. 3A, the UMPB approaches the

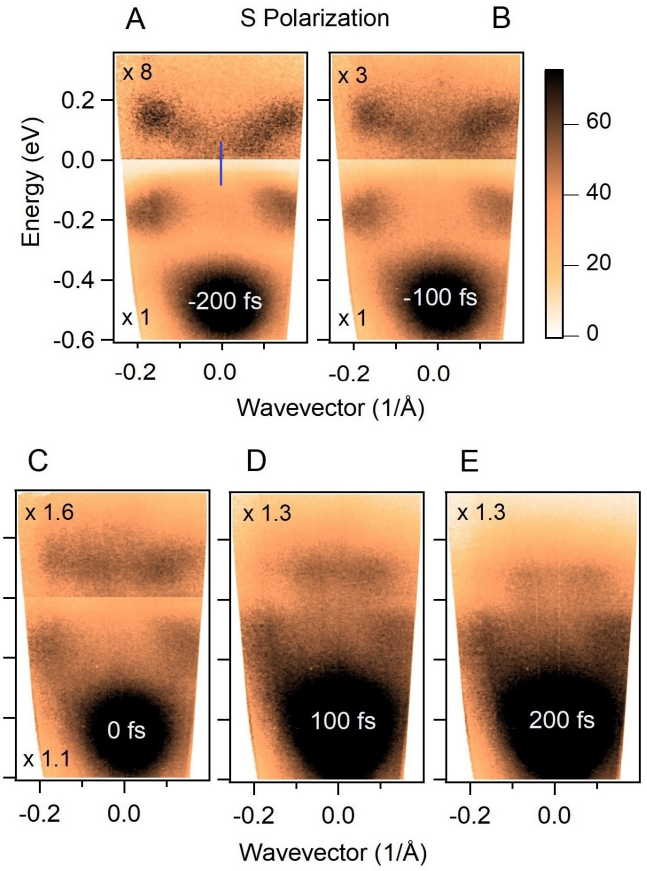

FIG. 3: A-E) Photoelectron intensity map acquired with ***S* probe polarization** along the $\overline{\Gamma} - \overline{M}$ direction for different pump-probe delays. The intensities above and below the Fermi level have been multiplied by rescaling factors in order to better visualize the electronic states with respect to a fixed color scale. The blue line in panel A stands for the electronic gap size.

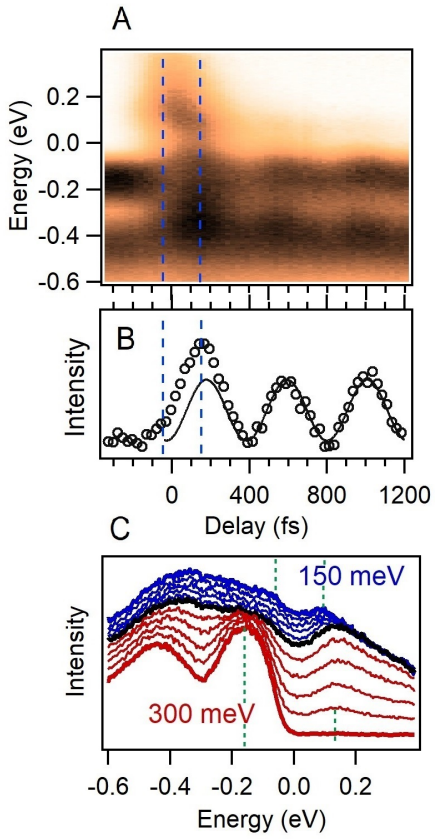

FIG. 4: A) Photoelectron intensity map acquired with ***S* probe polarization** at wavevector $k = 0.15$ Å^{-1} of the $\overline{\Gamma} - \overline{M}$ direction, as a function of pump-probe delay. B) Photoelectron intensity of panel A) integrated with the energy interval [-65,-85] meV, which is dominated by coherent displacement of the CDW amplitude. The solid line is a cosinus fit of the oscillations for $\tau > 400$ fs. C) Energy distribution curves extracted from the intensity map of panel A) for pump-probe delays $-300 < \tau < 150$ fs. Red curves correspond to $-300 < \tau < 0$ fs, the black curve is at $\tau = 0$, and blue curves are for $0 < \tau < 150$ fs.

LMPB towards the center of the SBZ, where their peak-to-peak energy distance becomes 0.15±0.1 eV. This value is near to the calculated $\Delta_L = 0.12$ eV, suggesting that L termination is likely the dominant one. Figure 3A shows an intensity map acquired on the rising tail of the pump pulse, namely when the observed UMPB is still representative of a weakly photoexcited state (at delay time of -200 fs, the leading tail of the probe pulse has a small but finite overlap with the pump pulse). It follows that Fig. 3A shows a map of electronic states during the initial stage of photoexcitation. Subsequently, the absorbed energy density increases with pump-probe delay, leading to a full gap collapse. The snapshots in Fig. 3A-E) indicate a complete restructuring of the electronic states, characterized by spectral weight transfer from the dispersive branches of the UMPB towards ingap states near the center of the SBZ. After 200 fs from the arrival of the pump pulse, the intensity map of Fig. 3E corresponds to states with low wavevector dispersion, due to the electronic localization in fluctuating nanodomains of the CDW[22].

It is instructive to compare the dynamics of the melting process with the period of the CDW amplitude. Figure 4A shows the temporal evolution of the ARPES intensity integrated around $k_{||} = 0.15$ Å^{-1}. Periodic oscillations of the LMPB can be followed by plotting the ARPES intensity around -70 meV (see Fig. 4B). The coherent CDW motion displays the evolution expected from the displacive excitation of the SD breathing mode: it does take off near zero delays (more precisely -30 fs) and oscillates as a cosinus[30] with a period of 410 fs. As shown in Fig. 4A, the UMPB and LMPB approach to each other during the first half period of the CDW amplitude oscillation, nearly following the CDW displacement. This effect can be quantified in Fig. 4C, which shows energy distribution curves extracted from Fig. 4A for different

pump-probe delays. At zero delay, the UMPB-LMPB distance is still close to the maximal value of 300 meV, while it reduces to 150 meV for a delay time of 150 fs.

Well before the reduction of gap magnitude, a midgap intensity grows up between LMPB and UMPB, reaching at zero delays already 80% of the maximal value. The appearance of midgap states on a timescale faster than the coherent lattice motion has always been a hallmark of Mott physics[19–22,28]. Nonetheless, the sudden rise of such strong CDW fluctuations seems to be a general aspect of ultrafast phase transitions[32–34]. In the case of 1T-TaS_2, we think that correlation effects and CDW order are tightly connected. Notice that $\overline{U}$ depends on the stacking order (see Fig. 1D) and is highly affected by variation of orbital filling. Similarly, the photoinduced CDW fluctuations should also be coupled to local reduction of Coulomb repulsion and can easily engender mid-gap states.

In conclusion, the C-CDW of 1T-TaS_2 is an insulator in which an out-of-plane dimerization and electronic correlations are highly entangled. Our self-consistent DFT+GOU calculations can correctly reproduce the spectral properties of this Mott-Peierls compound. New data acquired with S polarization of the probe protons show that electronic states near to the chemical potential loosen the wavevector dispersion during the CDW melting. This process indicates that photoinduced fluctuations partially disrupt the long-range order within half a period of the CDW amplitude mode. The midgap states develop on a faster timescale, presumably due to the concurrent effects of screened Coulomb repulsion and electronic correlations.

[1] J. A. Wilson, F. J. Di Salvo, and S. Mahajan, Advances in Physics **24**, 117 (1975).
[2] A. Spijkerman, J. L. de Boer, A. Meetsma, G. A. Wiegers and S. van Smaalen, Physical Review B **56**, 13757 (1997).
[3] L. Perfetti, T. A. Gloor, F. Mila, H. Berger, and M. Grioni, Physical Review B, **71** 153101 (2005).
[4] L. Perfetti, A. Georges, S. Florens, S. Biermann, S. Mitrovic, H. Berger, Y. Tomm, H. Höchst and M. Grioni, Physical Review Letters **90** 166401 (2003).
[5] S. Colonna, F. Ronci, A. Cricenti, L. Perfetti, H. Berger and M. Grioni, Physical Review Letters **94**, 036405 (2005).
[6] B. Sipos, A. F. Kusmartseva, A. Akrap, H. Berger, L. Forró and E. Tutis, Nature Materials **7**, 960 (2008).
[7] L. Stojchevska, I. Vaskivskyi, T. Mertelj, P. Kusar, D. Svetin, S. Brazovskii and D. Mihailovic, Science **334**, 177 (2014).
[8] I. Vaskivskyi, J. Gospodaric, S. Brazovskii, D. Svetin, P. Sutar, E. Goreshnik, I. A. Mihailovic, T. Mertelj and D. Mihailovic, Science Advances **1**, e1500168 (2015).
[9] D. Cho, S. Cheon, K.-S. Kim, S.-H. Lee, Y.-H. Cho, S.-W. Cheong and H. W. Yeom, Nature Communication **7**, 10453 (2016).
[10] Y. D. Wang, W. L. Yao, Z. M. Xin, T. T. Han, Z. G. Wang, L. Chen, C. Cai, Y. Li and Y. Zhang, Nature Communication **11**, 4215 (2020).
[11] T. Ritschel, J. Trinckauf, K. Koepernik, B. Büchner, M. V. Zimmermann, H. Berger, Y. I. Joe, P. Abbamonte, P. and J. Geck, Nature Physics **11**, 328 (2015).
[12] T. Ritschel, H. Berger, and J. Geck, Physical Review B **98**, 195134 (2018).
[13] S.-H. Lee, J. S. Goh, and D. Cho, Physical Review Letters **122**, 106404 (2019).
[14] C. J. Butler, M. Yoshida, T. Hanaguri, and Y. Iwasa, Nature Communication **11**, 2477 (2020).
[15] G. von Witte, T. Kisslinger, J. G. Horstmann, K. Rossnagel, M. A. Schneider, C. Ropers, and L. Hammer, Physical Review B **100**, 155407 (2019).
[16] S. Biermann, A. Poteryaev, A. I. Lichtenstein and A. Georges, Physical Review Letters **94**, 026404 (2005).
[17] D. Shin, N. Tancogne-Dejean, J. Zhang, M. S. Okyay, A. Rubio and N. Park, Physical Review Letters **126**, 196406 (2021).
[18] P. Fazekas and E. Tosatti, Philosophical Magazine B **39**, 229 (1979).
[19] L. Perfetti, P. A. Loukakos, M. Lisowski, U. Bovensiepen, H. Berger, S. Biermann, P. S. Cornaglia, A. Georges and M. Wolf, Physical Review Letters **97**, 067402 (2006).
[20] L. Perfetti, P. A. Loukakos, M. Lisowski, U. Bovensiepen, M. Wolf, H. Berger, S. Biermann and A. Georges, New Journal of Physics **10**, 053019 (2008).
[21] J. C. Petersen, S. Kaiser, N. Dean, A. Simoncig, H. Y. Liu, A. L. Cavalieri, C. Cacho, I. C. E. Turcu, E. Springate, F. Frassetto, L. Poletto, S. S. Dhesi, H. Berger, H. and A. Cavalleri, Physical Review Letters **107**, 177402 (2011).
[22] C. Sohrt, A. Stange, M. Bauer, and K. Rossnagel, Faraday Discussion **171**, 243 (2014).
[23] F. Petocchi, C. W. Nicholson, B. Salzmann, D. Pasquier, O. V. Yazyev, C. Monney, and P. Werner, Physical Review Letter **129**, 016402 (2022).
[24] A. S. Ngankeu, S. K. Mahatha, K. Guilloy, M. Bianchi, C. E. Sanders, K. Hanff, K. Rossnagel, J. A. Miwa, C. Breth Nielsen, M. Bremholm and P. Hofmann, Physical Review B **96**, 195147 (2017).
[25] J. Faure, J. Mauchain, E. Papalazarou, W. Yan, J. Pinon, M. Marsi and L. Perfetti, Review of Scientific Instruments **83**, 043109 (2012).
[26] J. Demsar, L. Forro, H. Berger, D. Mihailovic, Physical Review B **66**, 041101(R) (2002).
[27] A. Zong, X. Shen, A. Kogar, L. Ye, C. Marks, D. Chowdhury, T. Rohwer, B. Freelon, S. Weathersby, R. Li, J. Yang, J. Checkelsky, X. Wang and N. Gedik, Science Advances **4**, eaau5501 (2018).
[28] M. Ligges, I. Avigo, D. Golez, H. U. R. Strand, Y. Beyazit, K. Hanff, F. Diekmann, L. Stojchevska, M. Kalläne, P. Zhou, K. Rossnagel, M. Eckstein, P. Werner and U. Bovensiepen, Physical Review Letters **120**, 166401 (2018).
[29] S. W. Jung, S. H. Ryu, W. J. Shin, Y. Sohn, M. Huh, R. J. Koch, C. Jozwiak, E. Rotenberg, A. Bostwick and K. S. Kim, Nature Materials **19**, 277 (2020).
[30] E. Papalazarou, J. Faure, J. Mauchain, M. Marsi, A. Taleb-Ibrahimi, I. Reshetnyak, A. van Roekeghem, I. Timrov, N. Vast, B. Arnaud, L. Perfetti, Physical Review Letters **108**, 256808 (2012).
[31] Y. Chen, W. Ruan, M. Wu, S. Tang, H. Ryu, H.-Z. Tsai,

R. L. Lee, S. Kahn, F. Liou, C. Jia, O. R. Albertini, H. Xiong, T. Jia,Z. Liu, J. A. Sobota, A. Y. Liu, J. E. Moore, Z.-X. Shen, S. G. Louie, S.-K. Mo and M. F. Crommie, Nature Physics **16**, 218 (2020).

[32] A. Zong, A. Kogar, Y.-Q. Bie, T. Rohwer, C. Lee, E. Baldini, E. Ergeçen, M. B. Yilmaz, B. Freelon, E. J. Sie, H. Zhou, J. Straquadine, P. Walmsley, P. E. Dolgirev, A. V. Rozhkov, I. R. Fisher, P. Jarillo-Herrero, B. V. Fine and N. Gedik, Nature Physics **15**, 27 (2019).

[33] L. X. Yang, G. Rohde, K. Hanff, A. Stange, R. Xiong, J. Shi, M. Bauer, and k. Rossnagel, Physical Review Letters **125**, 266402 (2020).

[34] V. Brouet, J. Mauchain, E. Papalazarou, J. Faure, M. Marsi, P. H. Lin, A. Taleb-Ibrahimi, P. Le Fèvre, F. Bertran, L. Cario, E. Janod, B. Corraze, V. T. Phuoc and L. Perfetti, Physical Review B **87**, 041106(R) (2013).

[35] S. Duan, Y. Cheng, W. Xia, Y. Yang, C. Xu, F. Qi, C. Huang, T. Tang, T. Guo, W. Luo, D. Qian, D. Xiang, J. Zhang and W. Zhang, W. Nature **595**, 239 (2021).